A New Perspective of Wind Power Grid Codes Under Unbalanced and Distorted Grid Conditions

Islam, Md Moinul; Hossain, Eklas; Padmanaban, Sanjeevikumar; Brice, Charles W.

Published in:
IEEE Access

DOI (link to publication from Publisher):
10.1109/ACCESS.2020.2966907

Publication date:
2020

Document Version
Publisher's PDF, also known as Version of record

IEEE Access
Multidisciplinary | Rapid Review | Open Access Journal

Received January 2, 2020, accepted January 8, 2020, date of publication January 15, 2020, date of current version January 27, 2020.

Digital Object Identifier 10.1109/ACCESS.2020.2966907

A New Perspective of Wind Power Grid Codes Under Unbalanced and Distorted Grid Conditions

MD MOINUL ISLAM[1], (Member, IEEE), EKLAS HOSSAIN[2], (Senior Member, IEEE), SANJEEVIKUMAR PADMANABAN[3], (Senior Member, IEEE), AND CHARLES W. BRICE[4]

[1]Electric Reliability Council of Texas, Taylor, TX 76574, USA
[2]Department of Electrical Engineering and Renewable, Oregon Renewable Energy Center (OREC), Oregon Tech, Klamath Falls, OR 97601, USA
[3]Department of Energy Technology, Alborg University, 9220 Aalborg, Denmark
[4]Department of Electrical Engineering, University of South Carolina, Columbia, SC 29208, USA

Corresponding author: Eklas Hossain (eklas.hossain@oit.edu)

This work was supported in part by the National Science Foundation (NSF) Industry University Cooperative Research Center (I/UCRC) on Grid-connected Advanced Power Electronic Systems (GRAPES) under Grant 0934378.

ABSTRACT Increasing penetration of wind power has led power system operators worldwide to develop new grid codes for integration of a wind power plant (WPP) onto the grid. According to the grid codes issued by Federal Energy Regulatory Commission (FERC) in the US, a WPP must have low voltage ride through (LVRT) capability, power factor design criteria, and supervisory control and data acquisition (SCADA) system to ensure power system reliability. Fast Fourier transform (FFT) is frequently used to measure root mean square (RMS) voltage, power factor, and for supervisory data acquisition in order to verify that a WPP conforms to the grid code requirements. However, FFT inherently assumes signal is periodic in nature, and it provides misleading results under unbalanced and distorted grid conditions. To overcome these issues, this work proposes a new method for wind power grid codes based on time-frequency analysis technique. Unlike FFT, it provides accurate result both in steady-state and transient conditions. The efficacy of the proposed method is verified by applying it to computer simulated and real-world cases provided by National Renewable Energy Laboratory (NREL) in the US. Time-frequency analysis is performed utilizing Time-Frequency Toolbox (TFTB) in MATLAB® developed for the analysis of non-stationary signals.

INDEX TERMS Fast Fourier transform, grid codes, power systems, time-frequency distribution, wind power.

I. INTRODUCTION

This energy can play a significant role in alleviating increasing energy demands on the electrical grid. According to US Energy Information Administration (EIA), the total energy demand in the US is estimated to increase by 39% from 2005 to 2030 [1]. This increment will result in net energy demand to be 5.8 billion MWh by 2030. To meet 20% of this energy demand, US Department of Energy (DOE) aimed to integrate additional 300 GW wind power plants (WPPs) into the grid by 2030 [1]. This large-scale integration of WPPs may have harmful impacts on the grid as they are considered as intermittent power sources. Therefore, interconnection requirements for WPPs are developed worldwide to mitigate their negative impacts and protect power systems reliability [2]–[4]. In [5], [6], the studies suggested that it is ineluctable for various national and international organizations and personnel to investigate new grid codes or to update the present active grid standards for wide-scale penetration of renewable energy sources into the grid. In the US, the Federal Energy Regulatory Commission (FERC) sets forth requirements and grid codes specific to WPPs. FERC is the US federal agency that assists consumers in obtaining reliable, efficient and sustainable energy services through proper regulatory. The grid codes issued by the FERC for interconnection of WPPs in the US mainly focuses on low voltage ride through (LVRT) capability, power factor design criteria, reactive power capability, supervisory control and data acquisition (SCADA) system [7], [8]. The LVRT capability of a WPP has been heavily studied in recent years [9]–[11] considering unbalanced and distorted grid conditions. In order to enhance the LVRT capability of a WPP, low RMS voltage at the point of interconnection (POI) caused by a power system fault should be assessed accurately. Also,

The associate editor coordinating the review of this manuscript and approving it for publication was Zhen Li.

to ensure electric power system reliability and fulfill the grid codes, power factor and supervisory data acquisition of a WPP should be obtained precisely.

FFT-based method is commonly used to assess the power quantities such as RMS voltage, power factor, active and reactive power, and provide useful information for SCADA system of WPPs. The FFT requires the signal to be periodic in nature, and only provides accurate assessment in steady-state [13], [14]. However, a WPP may introduce low voltage at POI caused by a power system fault [9], [15]. Also, transients are introduced by WPPs when they are connected to or disconnected from the grid and by events as capacitors switching. Furthermore, harmonics are injected into the grid by variable speed WPPs due to the switching of power electronic converters. Therefore, from the electrical grid perspective, WPPs are perceived as fluctuating power sources, and can be best described as non-stationary, non-sinusoidal and unbalanced in nature [15], [16]. Under such conditions, signal becomes aperiodic, and frequency contents of the signal change with time as well. Hence, FFT-based method provides erroneous results in the presence of real world disturbances [17], [18]. Also, it cannot extract dynamic signature of the disturbance events since computation is performed in frequency domain only [19], [20]. Therefore, application of time-frequency analysis (TFA) is motivated for the study of non-stationary signals in electric power systems, as it provides more accurate assessment than the conventional FFT. Also, it has the capability to present simultaneous time and variable frequency information of non-stationary signals [13], [21]. TFA has been applied to several areas of power and energy systems such as in power electronics, detection and classification of power-quality (PQ) disturbances [19], and mechanical fault detection in induction motors [19]–[21]. The application of TFA in wind power has been demonstrated in the research work of [17], [18], [21]. However, assessment of RMS voltage, power factor, and data acquisition for supervisory control system under unbalanced and distorted conditions in accordance with wind power grid codes have not been studied in these works. Also, in [17], [18], [21] TFA-based instantaneous THD is employed for the analysis of wind power impacts on the grid. The method defines THD based on the energy ratio of fundamental and harmonic components instead of the RMS values. Nonetheless, [17], [18], [21] provide inaccurate assessments of wind power impacts on the grid [13].

Regarding aforementioned issues, in this work, a new method is proposed for the analysis of wind power grid codes based on TFA. This paper contributes by overcoming the limitation of conventional FFT method that cannot provide time information of a disturbance introduced by a WPP. With the help of redefined power components such as RMS voltage and current, power factor, active and reactive power, the proposed methods are justified with computer simulated case studies for wind power grid codes under unbalanced and distorted grid conditions. It is seen that TFA-based redefined power components provide much more accurate results than the conventional FFT under unbalanced and distorted grid conditions. The proposed methods are then applied to three real-world case studies-voltage sag, transients and oscillatory type disturbances for instantaneous verification of wind power grid codes and data acquisition for SCADA system. Five years of recorded data indicate that these disturbances occurred on several occasions in 150 MW Trent Mesa WPP in Texas. This work demonstrates the impacts of these disturbances into the grid in details from reliability perspectives. Providing instantaneous direction of active and reactive power flow, the paper detects large amount of reverse power flow from grid to the Trent Mesa WPP during voltage sag that may cause mechanical damage of wind generating units in the plant. The time-varying resonant frequency component that is responsible for oscillatory type disturbances recorded in Trent Mesa WPP are identified and harmonics pollution injected by the WPP into the grid under normal and distorted grid conditions are shown.

The paper is organized as follows: Sec. II summarizes the wind power grid codes in the US. Sec. III introduces TFA method and discusses advantage of the method over conventional FFT. Next, power components are redefined for wind power grid codes under unbalanced and distorted grid conditions in Sec. IV. In Sec. V, superiority of the TFA-based redefined power components over FFT is demonstrated by applying them to computer simulated case studies. TFA based proposed method is then applied to real-world case studies for the analysis of wind power grid codes in Sec. VI. Finally, conclusions are drawn in Sec. VII.

II. OVERVIEW OF WIND POWER GRID CODES IN THE US

The electrical power grid in the US has three primary regions as shown in Fig. 1: the Western Interconnection, the Eastern Interconnection, and the Texas Interconnection. Seven independent system operators (ISOs) and regional transmission operators (RTOs) operate in these three interconnected regions according to North American Electric Reliability Corporation (NERC) standard to make sure reliability of bulk electric power systems [26]. NERC became certified Electric Reliability Organization (ERO) for the US by an order issued by FERC following the Northeast blackout of 2003 [12]. Prior to that, compliance to NERC's standard was highly encouraged but not mandatory.

In addition to NERC compliance, with increased penetration of wind energy in the US, FERC issued wind power grid code requirements that all small (less than or equal 20 MW) and large (more than 20 MW) WPPs must conform to. The grid codes issued by FERC for WPPs in the US are summarized as follows [7], [8]:

1. Low voltage ride through (LVRT) capability: The first grid code focuses on the LVRT capability of a WPP. The LVRT capability of wind turbine generators is the ability to operate through periods of lower grid voltage. As seen in the LVRT curve provided in Fig. 2, the two key aspects of this regulation are - a WPP must have the LVRT capability down to 15% of the rated line voltage for 0.625 s, and must be

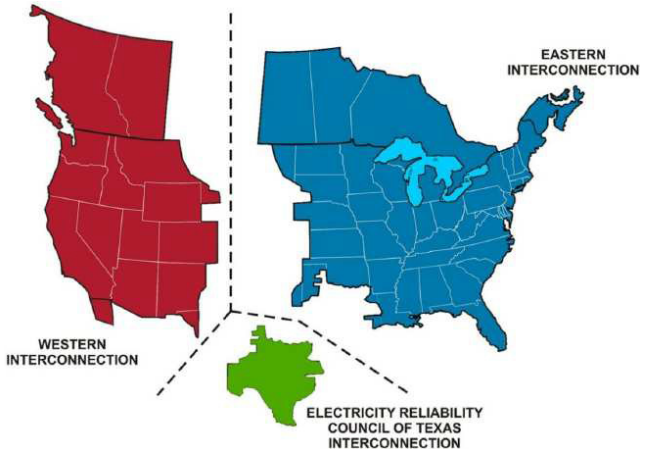

FIGURE 1. Map of the North American electricity interconnections [22].

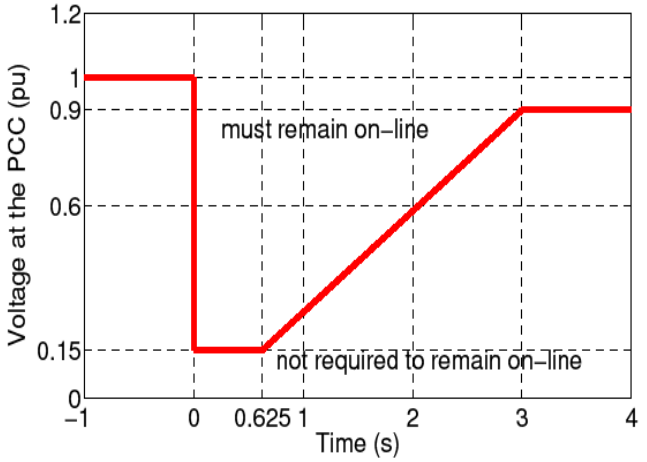

FIGURE 2. Low voltage ride through curve by FERC showing that a wind plant must have the ride through capability to 0.15 pu for 0.625 s while it must remain on-line at 0.9 pu.

able to operate continuously at 90% of the rated line voltage, measured at the high voltage side of the WPP substation transformer(s) [7].

2. Power Factor Design Criteria: According to the second grid code, the power factor of a synchronous or non-synchronous wind generating facility shall remain within the range of 0.95 leading to 0.95 lagging measured at the point of interconnection (POI) in order to ensure electric power system safety and reliability. Also, this power factor range shall be dynamic, and if necessary power electronic devices such as fixed and switched capacitors, or a combination of both can be used to deliver this level of reactive capability [7], [8].

3. Supervisory Control and Data Acquisition: To ensure system reliability, the WPP should have supervisory control and data acquisition (SCADA) system to transmit data and receive instructions from the transmission provider [7]. To comply with FERC grid code requirements, seven ISOs have their own protocols or planning criteria that all WPPs must fulfill for reliable power flow. The studied WPP in this work is located in Texas area and operates under ISO Electrical Reliability Council of Texas (ERCOT). All WPPs must provide a real-time SCADA point that will communicate to ERCOT and provide number of wind turbine generators (WTGs) that are available for active and/or reactive power injection into the ERCOT transmission grid. Also, there must be two other real-time SCADA points to provide the number of WTGs that are not able to communicate and out of service [25].

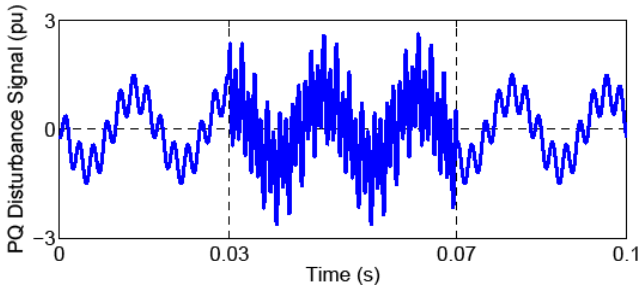

FIGURE 3. A non-stationary signal comprised of 60 Hz, 7th, and time-varying 15th harmonic component.

4. Harmonic: ERCOT requires all WPPs to comply with IEEE Std. 519 as mentioned in the technical report published by National Renewable Energy Laboratory (NREL) in the US [24], [27].

5. Reactive Power: All WPPs above 20 MVA must be able to deliver or absorb reactive power within the range of −32.8% to +32.8% of net active power output at POI (equivalent to 0.95 power factor) to maintain set point voltage profile by ERCOT. The voltage profile set by ERCOT might be different depending on the location and transmission voltage, typically it lies in between 0.95 to 1.05 pu for steady-state condition. In addition, ERCOT requires all WPPs shall be available to deliver reactive power at all MW output levels at or above 10% of their nameplate capacity. If MW output of a WPP is less than 10% of its nameplate capacity and it is unable to provide voltage support, ERCOT may require WPP to disconnect from the system to protect system reliability [25], [27].

Other countries such as Canada, China, Denmark, Germany, UK etc. have their own grid codes for WPPs and may differ from the grid code requirements discussed above. In this work, we focus on wind power grid codes in the US only. Summary of WPPs grid code requirements in other countries can be found in [2].

III. TIME-FREQUENCY ANALYSIS TECHNIQUE FOR WIND POWER GRID CODES

WPPs are considered as intermittent power sources. Therefore, application of time-frequency analysis (TFA) in wind power is motivated as it overcomes the limitations of conventional FFT method in case of non-stationary signals. For example, Fig. 3 represents a non-stationary signal that is

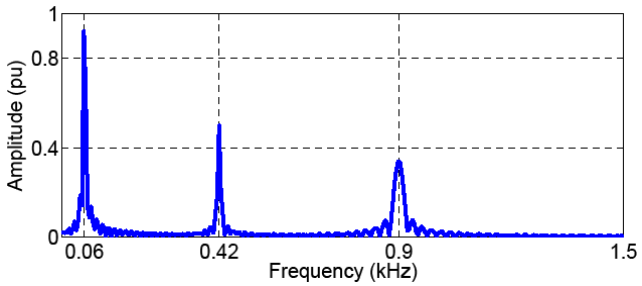

FIGURE 4. FFT of the non-stationary signal delineating the presence of 60 Hz, 7th, and 15th harmonic components in the signal.

comprised of 60 Hz and 7th harmonic, and a time-varying 15th harmonic component that persists in the signal from 0.03 s to 0.07 s.

Fig. 4 represents FFT of the signal and illustrates the presence of 60 Hz, 7th, and 15th harmonic components in the signal. However, it does not provide any information about what time these frequency components appear and how long they exist in the signal. Also, side lobes are observed around these frequency components due to spectral leakage. These side lobes cause inaccurate assessment in FFT-based method. On the other hand, time-frequency distribution (TFD) of the signal in Fig. 5 provides both time and frequency information. From the figure, it is observed that the time-varying 15th harmonic component appears at 0.03 s and exists till 0.07 s. The color bar in the figure indicates energy of the frequency components in time-frequency domain, where red color indicates the highest energy and blue color refers to the lowest energy of the frequency components in the signal. Therefore, 60 Hz frequency component has the highest energy, and the time-varying 15th harmonic has the lowest energy in the signal, respectively. Note that in signal processing energy is defined as $\boldsymbol{E} = |\boldsymbol{x}(\boldsymbol{t})|^{\boldsymbol{2}}$, where $\boldsymbol{x}(\boldsymbol{t})$ is a time-domain signal and E is energy of the signal. Therefore, 60 Hz has the highest magnitude and time-varying 15th harmonic has the lowest magnitude in the signal based on their energy distribution in Fig. 5. Since, TFD shows suitable properties and overcomes the limitations of the conventional FFT method, in this work the TFD method for the analysis of wind power grid codes under unbalanced distorted grid conditions is employed.

Several TFD methods such as Wigner-Ville (WV), Spectrogram, reduced interference distribution (RIDB), Choi Wiliams, Zhao-Altas-Marks (ZAM), Born-Jordan (BJ), Page, etc. can be used for time-frequency analysis. L. Cohen first generalized all TFDs as [18]:

$$\boldsymbol{TFD_v}\,(\boldsymbol{t},\boldsymbol{\omega};\phi) = \frac{\boldsymbol{1}}{\boldsymbol{4\pi^2}} \iiint \boldsymbol{v}^{*}\left(\boldsymbol{u}-\frac{\boldsymbol{\tau}}{\boldsymbol{2}}\right)\boldsymbol{v}\left(\boldsymbol{u}+\frac{\boldsymbol{\tau}}{\boldsymbol{2}}\right)\boldsymbol{\phi}\,(\boldsymbol{\theta},\boldsymbol{\tau}) \times \boldsymbol{e}^{-\boldsymbol{j\theta t}-\boldsymbol{j\tau\omega}+\boldsymbol{j\theta u}}\boldsymbol{d\theta d\tau du} \quad (1)$$

where $\boldsymbol{v}(\boldsymbol{t})$ is the analytic (complex) representation of a signal, and $\boldsymbol{v}^{*}(\boldsymbol{t})$ is the complex conjugate of $\boldsymbol{v}(\boldsymbol{t})$. The variable $\boldsymbol{\theta}$ represents a frequency domain shift and $\boldsymbol{\tau}$ a time domain shift. The function $\boldsymbol{\phi}\,(\boldsymbol{\theta},\boldsymbol{\tau})$ is known as a kernel which is

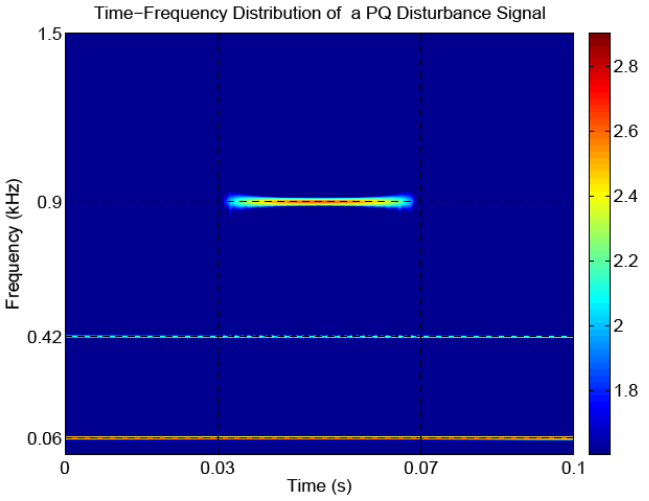

FIGURE 5. Time-frequency distribution of the non-stationary signal comprised of 60 Hz, 7th, and time-varying 15th harmonic components that persists in the signal from 0.03s to 0.07s.

basically a two dimensional low pass filter employed in the time-frequency domain in order to minimize the interference terms.

In the definition of $\boldsymbol{TFD_v}\,(\boldsymbol{t},\boldsymbol{\omega};\boldsymbol{\phi})$, time variable t and frequency variable $\boldsymbol{\omega}$ represent a signal in time and frequency-domain as illustrated in Fig. 3. Whereas, FFT represents a signal in the frequency-domain only according to [18] as follows:

$$\boldsymbol{V}\,(\boldsymbol{\omega}) = \frac{1}{\sqrt{2}}\int \boldsymbol{v}\,(\boldsymbol{t})\,\boldsymbol{e}^{-\boldsymbol{j\omega t}}\boldsymbol{dt} \quad (2)$$

Due to the absence of time variable t in the definition of FFT, it cannot represent a signal in time-domain compared to TFA as observed in Fig. 4. However, interference terms are introduced in time-frequency domain as a result of byproduct of the self-conjugate terms $\boldsymbol{v}\left(\boldsymbol{u}+\frac{\boldsymbol{\tau}}{\boldsymbol{2}}\right)\boldsymbol{v}^{*}\left(\boldsymbol{u}-\frac{\boldsymbol{\tau}}{\boldsymbol{2}}\right)$ in (1). These interference terms show energy content of unnecessary frequency components that actually do not exist in the signal and result in inaccurate assessment. Among all TFDs, RIDB shows the most suitable properties to minimize the interference terms [13], [17], [18]. Therefore, in this work, RIDB is chosen for the analysis of wind power grid codes under unbalanced and distorted grid conditions. Also, TFA is a bilinear transform since signal appears twice as seen in the definition of TFD in (1). As a result, it suffers from high computational complexity. Therefore, it is necessary to eliminate unnecessary data so that less amount of data is processed at SCADA center employing the proposed TFA method. Appropriate data with accuracy can be processed for SCADA system by identifying key nodes for potential voltage collapse, cascading failure and other instability issues in power systems. The critical nodes can be identified by employing ac power flow analysis, state estimation technique, event-trigger particle filter and heterogeneous nonlinear filter etc. in smart grid and wide area management systems [19]–[22].

The self-conjugate terms $v\left(u+\frac{\tau}{2}\right)v^*\left(u-\frac{\tau}{2}\right)$ in (1) basically provide energy information $|v(t)|^2$ of the signal $v(t)$. Based on the energy information one can acquire RMS value of $v(t)$ as [13]:

$$V^{TFA}=\frac{1}{\sqrt{2}}\sqrt{\frac{1}{T}\int_o^T TFD_v\left(t,\omega;\phi\right)} \tag{3}$$

where T is the fundamental period.

Scale factor $\frac{1}{\sqrt{2}}$ is incorporated in (2) due to energy of the original signal being half of the analytic signal [18]. As discussed above, Cohen's class TFDs provide energy information of a signal. Based on the energy information, one can assess RMS voltage and current according to (2). However, it cannot provide active and reactive power information for a pair of voltage and current signals. To obtain active and reactive power under unbalanced and distorted grid conditions, the self-conjugate terms in (1) are replaced by a pair of voltage and current signals as $v\left(u+\frac{\tau}{2}\right)i^*\left(u-\frac{\tau}{2}\right)$. The state of the art is known as cross time-frequency distribution (CTFD), and defined as [13]:

$$CTFD_{vi}\left(t,\omega;\phi\right)=\frac{1}{4\pi^2}\iiint v\left(u+\frac{\tau}{2}\right)i^*\left(u-\frac{\tau}{2}\right)\times\phi\left(\theta,\tau\right)e^{-j\theta t-j\tau\omega+j\theta u}d\omega d\tau du \tag{4}$$

Thus, CTFD represents complex power in time-frequency domain, and real part and imaginary part of the CTFD provide active and reactive power information for a pair of voltage and current signals, respectively. Employing the CTFD, average active and reactive power under unbalanced and distorted grid conditions can be obtained as follows [13]:

$$P^{TFA}=\frac{1}{2T}\int_o^T\Re\{CTFD_{vi}\left(t,\omega;\phi\right)\} \tag{5}$$

$$Q^{TFA}=\frac{1}{2T}\int_o^T\Im\{CTFD_{vi}\left(t,\omega;\phi\right) \tag{6}$$

Scale factor $\frac{1}{2}$ is incorporated in (4) and (5) as power of the original signal being half of the analytic signal [13]. Based on TFA discussed above, a set of indices are redefined in the next section that are utilized to verify wind power grid codes. Also, to obtain data for supervisory control system under unbalanced and distorted grid conditions.

IV. TFA-BASED INDICES FOR WIND POWER GRID CODES

The IEEE Std. 1459-2010 defines a set of power components such as effective RMS voltage and current, effective power factor, positive sequence active and reactive power, harmonic power, effective apparent power etc. under non-sinusoidal and unbalanced conditions [24]. These indices are defined based on conventional FFT method. As discussed earlier, FFT may result in inaccurate assessment of these power indices under unbalanced and distorted grid conditions. Hence, they are redefined based on the proposed TFA method to obtain accurate assessment for the analysis of wind power grid codes in the following manner.

A. TFA-BASED EFFECTIVE RMS VOLTAGE

The first grid code which provides information about LVRT capability can be verified by defining the effective RMS voltage V_e under unbalanced and distorted conditions according to the IEEE Standard 1459-2010 [24] as follows:

$$V_e=\sqrt{\frac{\left(V_a^{TFA}\right)^2+\left(V_b^{TFA}\right)^2+\left(V_c^{TFA}\right)^2}{3}} \tag{7}$$

where V_a^{TFA}, V_b^{TFA} are V_c^{TFA} TFA-based effective RMS voltage of the corresponding phase that can be calculated using (2).

B. TFA-BASED EFFECTIVE POWER FACTOR

The second grid code emphasizes on WPP power factor requirement and can be verified by defining the effective power factor PF_e under unbalanced and distorted conditions based on the TFA method as follows [24]:

$$PF_e=\frac{P}{S_e}=\frac{P}{3\cdot V_e\cdot I_e} \tag{8}$$

where

$$I_e=\sqrt{\frac{\left(I_a^{TFA}\right)^2+\left(I_b^{TFA}\right)^2+\left(I_c^{TFA}\right)^2}{3}} \tag{9}$$

$$P=P_a^{TFA}+P_b^{TFA}+P_c^{TFA} \tag{10}$$

where I_e and P are effective RMS current and total active power of the WPP and can be obtained via (2) and (4), respectively.

C. TFA-BASED DATA ACQUISITION FOR SCADA SYSTEM

SCADA system in a WPP is used to access and monitor data in real-time to carry out any kind of comparative analysis and take necessary steps to protect power systems reliability. For analysis and monitoring purpose of a WPP data, in this work, voltage and current THDs, active power, apparent power, reactive power and harmonic pollution information for the SCADA system are obtained employing the proposed TFA method.

1) EQUIVALENT TOTAL HARMONIC DISTORTION

THD is the commonly used power quality factor to quantify harmonics injection into the grid by a variable speed WPP. The equivalent voltage THD_{eV} and current THD_{eI} for a variable speed WPP can be assessed as [24]:

$$THD_{eV}=\frac{V_{eH}^{TFA}}{V_{e1}^{TFA}};\quad THD_{eI}=\frac{I_{eH}^{TFA}}{I_{e1}^{TFA}} \tag{11}$$

where V_{e1}, V_{eH} and I_{e1}, I_{eH} are TFA-based effective fundamental and harmonics RMS voltage and current, respectively. Harmonics and fundamental frequency components are separated employing the signal decomposition method in [13], [17], [18]. This index is used to check if WPP complies with IEEE Std. 519 as part of grid code requirements.

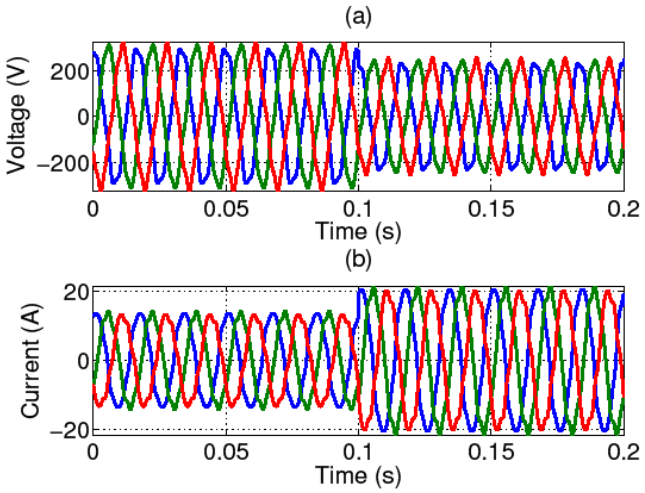

FIGURE 6. Simulation employing both FFT and TFA methods for the non-stationary, non-sinusoidal and unbalanced three-phase (a) voltage sag, and (b) current signals.

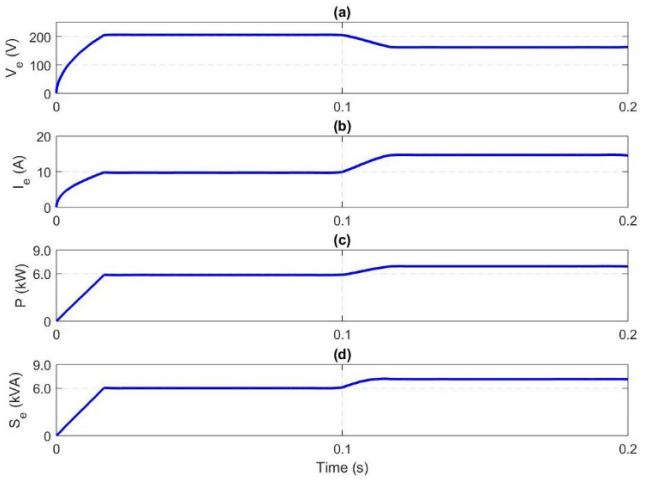

FIGURE 7. Transient response of (a) effective rms voltage V_e, (b) effective rms current I_e, (c) total active power P, and (d) effective apparent power S_e during the voltage sag that occurs at t = 0.1 s.

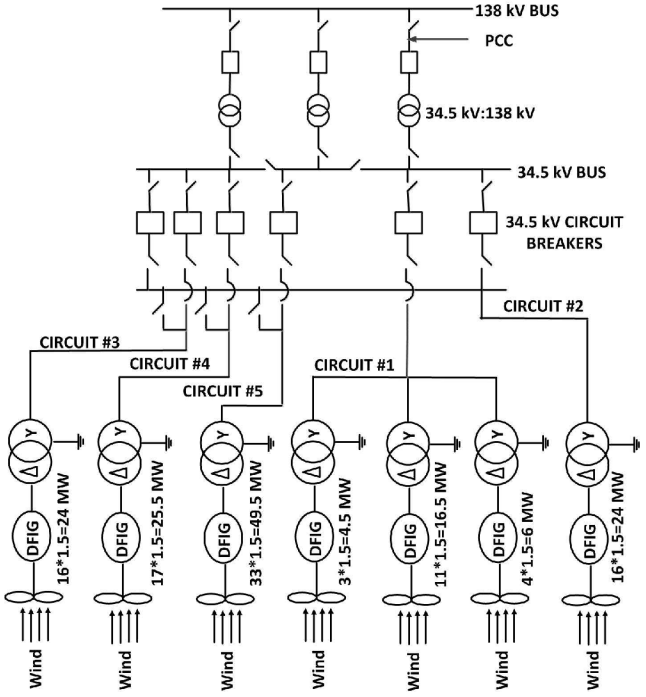

FIGURE 8. Simplified one-line diagram of 150 MW Trent Mesa wind power plant.

2) ACTIVE POWER

The positive sequence active power $\boldsymbol{P_1^+}$, harmonic active power $\boldsymbol{P_H}$, and the total active power P of a WPP are obtained as [24]:

$$\boldsymbol{P_1^+ = \frac{1}{2T}\int_o^T R\left\{CTFD_{v_1^+ i_1^+}(t,\omega;\phi)\right\}} \tag{12}$$

$$\boldsymbol{P_H = P_{aH}^{TFA} + P_{bH}^{TFA} + P_{cH}^{TFA}} \tag{13}$$

$$\boldsymbol{P = P_a^{TFA} + P_b^{TFA} + P_c^{TFA}} \tag{14}$$

where $\boldsymbol{P_{aH}^{TFA}, P_{bH}^{TFA}, P_{cH}^{TFA}}$ and $\boldsymbol{P_a^{TFA}, P_b^{TFA}, P_c^{TFA}}$ are obtained via CTFD of the harmonic and phase voltage and current signals, respectively. Index P provides total active power information that can be used to justify if a WPP delivers minimum 10% of its rated capacity according to ERCOT requirement. In addition, it can be used to determine if there is any reverse power flow under abnormal grid conditions.

3) REACTIVE POWER

The most suggested reactive power expression is the fundamental positive sequence reactive power [24] which is defined as:

$$\boldsymbol{Q_1^+ = \frac{1}{2T}\int_o^T \Re\left\{CTFD_{v_1^+ i_1^+}(t,\omega;\phi)\right\}} \tag{15}$$

This index provides instantaneous reactive power information, and is used to verify if a WPP is able to deliver or absorb defined reactive power (32.8% of net active power) to maintain set point voltage profile that lies between 0.95 pu to 1.05 pu according to ERCOT requirement.

4) APPARENT POWER

The TFA-based effective harmonic apparent power $\boldsymbol{S_{eH}}$, non-fundamental apparent power $\boldsymbol{S_{eN}}$, and total apparent power $\boldsymbol{S_e}$, [24] for a WPP are defined as:

$$\boldsymbol{S_{eH} = S_{e1}^{TFA} \cdot THD_{eV} \cdot THD_{eI}} \tag{16}$$

$$\boldsymbol{S_{eN} = S_{e1}^{TFA} \cdot \sqrt{THD_{eV}^2 + THD_{eI}^2 + THD_{eV} \cdot THD_{eI}}} \tag{17}$$

$$\boldsymbol{S_e = \sqrt{S_{e1}^2 + S_{eN}^2}} \tag{18}$$

5) HARMONIC POLLUTION

In this work, a variable speed type 3 (DFIG) WTG is studied that injects harmonics into the grid due to the switching of partial scale frequency converter. To obtain harmonic pollu-

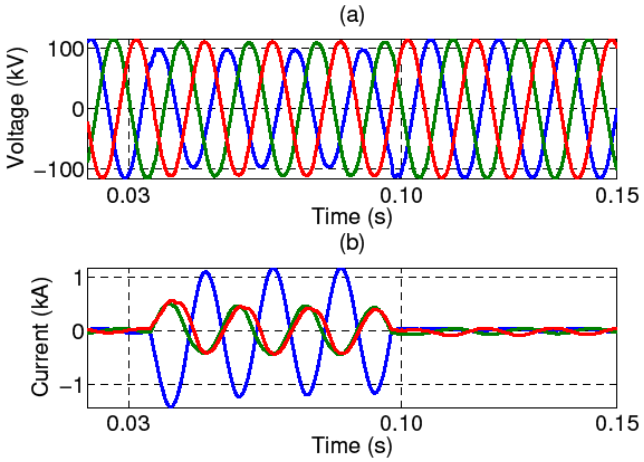

FIGURE 9. (a) Voltage sag, and (b) corresponding current signal recorded from TRENT Mesa WPP in Texas, US.

tion injected by the studied WPP, harmonic pollution index in [24] is refined based TFA as:

$$HP = \frac{S_{eN}}{S_{e1}} \tag{19}$$

The above TFA-based redefined indices in (7) – (19) are quantified as a single value based on (3), (5) and (6), and compared them to the classical FFT method as discussed in next section. Also, to obtain dynamic signature of these indices in (7) – (19) under distorted grid conditions, the instantaneous RMS voltage, active and reactive power are assessed over a moving window of one fundamental cycle in the following manner:

$$V^{TFA}(t) = \frac{1}{\sqrt{2}}\sqrt{\frac{1}{T}\int_{t-T}^{t}\int_{\omega} TFD_v(t,\omega;\phi)\,d\omega dt} \tag{20}$$

$$P^{TFA}(t) = \frac{1}{2T}\int_{t-T}^{t}\int_{\omega} R\{CTFD_{vi}(t,\omega;\emptyset)\}d\omega dt \tag{21}$$

$$Q^{TFA}(t) = \frac{1}{2T}\int_{t-T}^{t}\int_{\omega} I\{CTFD_{vi}(t,\omega;\emptyset)\}d\omega dt \tag{22}$$

Note that TFA-based instantaneous indices take one cycle to reach in steady-state following a disturbance since they are quantified over a moving window of one fundamental cycle.

V. SIMULATED CASE STUDY

In this section, both steady-state and non-stationary, non-sinusoidal and unbalanced cases are considered to justify efficacy of the TFA-based proposed method over conventional FFT. In this study, computer simulated signals are considered for a fair comparison for having a prior knowledge of the voltage and current signals. The results are discussed and summarized in the following subsections.

A. STEADY-STATE, NONSINUSOIDAL AND UNBALANCED CASE STUDY

In this case study, following computer simulated three-phase steady-state, non-sinusoidal and unbalanced voltage signals

TABLE 1. Comparison of FFT and TFA under steady-state, non-sinusoidal and unbalanced case study.

Indices	Actual	FFT	TFA	|% Error| in FFT	|% Error| in TFA
V_e (pu)	1.0677	1.0675	1.0674	0.0187	0.0281
PF_e	0.9369	0.9359	0.9364	0.1067	0.0534
THD_V (pu)	0.1801	0.1786	0.1789	0.8329	0.6663
THD_I (pu)	0.2271	0.2268	0.2269	0.1321	0.0881
P_1^+ (pu)	2.9811	3.002	3.009	0.7011	0.9359
P_H (pu)	0.0081	0.008161	0.008165	0.7531	0.8025
P (pu)	2.9295	2.9319	2.9321	0.0819	0.0888
S_{eH} (pu)	0.1259	0.12603	0.12601	0.1033	0.0874
S_{eN} (pu)	1.0593	1.0598	1.0599	0.0472	0.0566
S_e (pu)	3.1274	3.1309	3.1292	0.1119	0.0576
Q_1^+ (pu)	0.3910	0.3946	0.3945	0.9207	0.8951
HP (pu)	0.3534	0.3543	0.3542	0.2547	0.2264

are considered:

$$\begin{aligned} v_a(t) &= 1\sqrt{2}\cos(\omega_1 t - 0.74^\circ) \\ &\quad +0.2\sqrt{2}\cos(\omega_3 t\ \mathcal{C}\ 6.76^\circ) \\ &\quad +0.1\sqrt{2}\cos(\omega_5 t - 142.3^\circ) \end{aligned} \tag{23}$$

$$\begin{aligned} v_b(t) &= 1.1\sqrt{2}\cos(\omega_1 t - 121.2^\circ) \\ &\quad +0.15\sqrt{2}\cos(\omega_3 t\ \mathcal{C}\ 6.28^\circ) \\ &\quad +0.05\sqrt{2}\cos(\omega_5 t\ \mathcal{C}\ 167.4^\circ) \end{aligned} \tag{24}$$

$$\begin{aligned} v_c(t) &= 1.05\sqrt{2}\cos(\omega_1 t - 121.3^\circ) \\ &\quad +0.1\sqrt{2}\cos(\omega_3 t\ \mathcal{C}\ 9.7^\circ) \\ &\quad +0.15\sqrt{2}\cos(\omega_5 t\ \mathcal{C}\ 157.7^\circ) \end{aligned} \tag{25}$$

And, the current signals are

$$\begin{aligned} i_a(t) &= 1\sqrt{2}\cos(\omega_1 t - 22^\circ) + 0.25\sqrt{2}\cos(\omega_3 t\,\mathcal{C}\,120^\circ) \\ &\quad +0.2\sqrt{2}\cos(\omega_5 t - 175^\circ) \end{aligned} \tag{26}$$

$$\begin{aligned} i_b(t) &= 0.95\sqrt{2}\cos(\omega_1 t - 120.8^\circ)\ 0.15\sqrt{2}\cos \\ &\quad (\omega_3 t\ \mathcal{C}\ 99.49^\circ) + 0.1\sqrt{2}\cos(\omega_5 t\ \mathcal{C}\ 65.09^\circ) \end{aligned} \tag{27}$$

$$\begin{aligned} i_c(t) &= 0.9\sqrt{2}\cos(\omega_1 t - 120.3^\circ) + 0.01\sqrt{2} \\ &\quad \cos(\omega_3 t\,\mathcal{C}\,100.01^\circ) + 0.05\sqrt{2}\cos(\omega_5 t\,\mathcal{C}\,57.7^\circ) \end{aligned} \tag{28}$$

The non-sinusoidal and unbalanced voltage and current signals in (23)-(28) are in steady-state, and periodic in nature. The performance of FFT and TFA under the case study is summarized in Table 1. As seen in the table, percentage errors associated with both methods are less than 1%, and close to actual values. In the steady-state case study, FFT is very competitive to the proposed TFA method, since signals are periodic, and no spectral leakage occurs in the assessment of FFT. However, significant performance difference is observed in between FFT and TFA in case of nonstationary and unbalanced signals as illustrated in next subsection.

B. NON-STATIONARY, NON-SINUSOIDAL AND UNBALANCED CASE STUDY

In reality, WPPs are considered as intermittent power sources. Hence, voltage and current signals are not stationary and

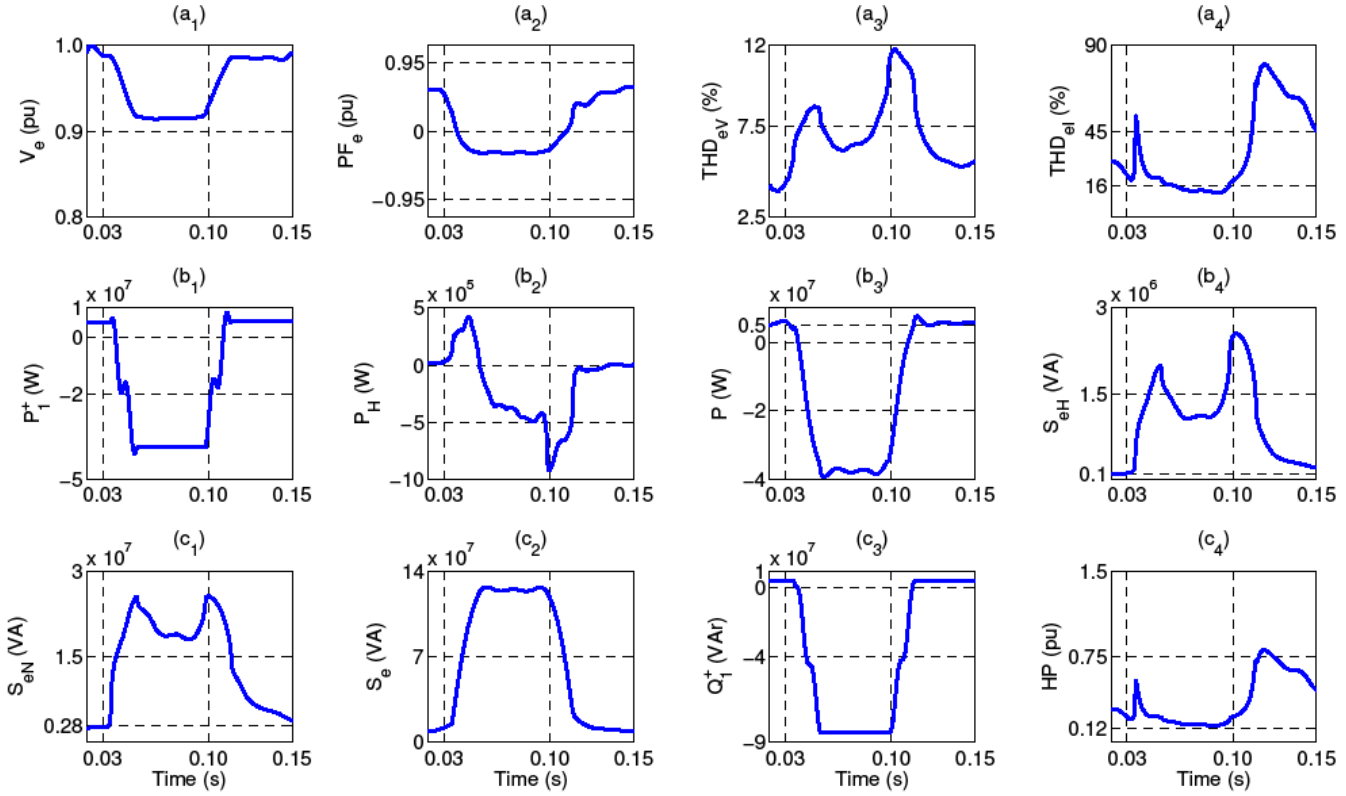

FIGURE 10. Results of voltage sag case study analysis based on the proposed TFA technique for wind power grid codes in the US.

periodic. Therefore, FFT-based method results in incorrect assessment of the indices for wind power grid codes due to spectral leakage phenomenon. To illustrate this further, these indices are measured employing both FFT and TFA methods for the non-stationary, non-sinusoidal and unbalanced voltage sag in Fig. 6. The results summarized in Table 2 justify that percentage error associated with FFT-based method is much higher than the proposed TFA method. The percentage error in case of FFT is more than 5% except for voltage and current THD. Whereas percentage error in TFA-based assessment of these indices is less than 2% only.

TFA provides better performance than FFT in case of aperiodic electrical signal under unbalanced and distorted grid conditions. Since it has inherent auto correlation (correlation of same electrical signal) and cross correlation (correlation of two different electrical signals) functions as observed in (1) and (4), respectively that do not require signal to be periodic in nature. Therefore, unlike FFT spectral leakage does not occur in TFA if a signal is aperiodic or non-stationary. In addition, in case of TFA, interference terms (unwanted frequency components) are filtered out employing a two dimensional low-pass filter $\varphi(\theta, \tau)$ as incorporated in (1) and (4). That also enhances the performance of TFA in assessment of both periodic and aperiodic signals. Also, transient response of these indices cannot be obtained via FFT due to lack of time information inherent in it. Whereas, transient response of these indices are obtained according to (20)-(22) employing TFA. As example, transient response of TFA-based instantaneous indices V_e, I_e, P, and S_e are incorporated in Fig. 7 that demonstrates the change in these indices before and after the voltage sag that occurs at t = 0.1 s. Following the sag, these indices take one cycle to reach in steady-state since they are assessed over a moving wind of one cycle t = 0.0167 s for the 60 Hz signals. Since, TFA provides much better accuracy and dynamic response of the system compared to classical FFT, in this work, TFA method is employed for wind power grid codes under

TABLE 2. Comparison of FFT and TFA under non-stationary, non-sinusoidal and unbalanced case study.

Indices	Actual	FFT	TFA	|% Error| in FFT	|% Error| in TFA
V_e (kV)	0.1855	0.2059	0.1845	10.9973	0.5391
PF_e	0.9221	0.9692	0.9218	5.1079	0.0325
THD_V (pu)	0.0752	0.0768	0.076	2.1277	1.0638
THD_I (pu)	0.0761	0.0773	0.0757	1.5769	0.5256
P_1^+ (kW)	6.2698	6.6571	6.1597	6.1772	1.7560
P_H (kW)	0.0004	0.000454	0.000399	15.2284	1.2690
P (kW)	6.3965	6.9593	6.321	8.7986	1.1803
S_{eH} (kVA)	0.003946	0.004484	0.003944	13.6341	0.0507
S_{eN} (kVA)	0.7389	0.8119	0.7344	9.8796	0.6090
S_e (kVA)	6.9371	7.8389	6.9967	12.9997	0.8591
Q_1^+ (kVar)	2.2571	2.4376	2.2394	7.9970	0.7842
HP (pu)	0.1071	0.1196	0.1078	11.6713	0.6536

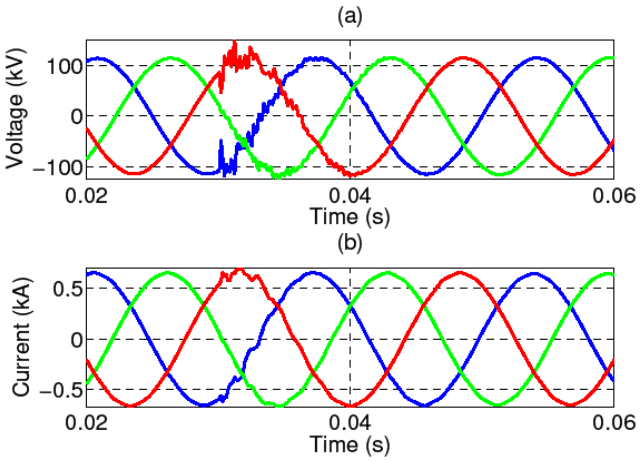

FIGURE 11. (a) Transient voltage, and (b) corresponding current signal recorded from TRENT Mesa WPP in Texas, US.

TABLE 3. Parameters of GE 1.5 MW DFIG wind turbine generator.

DFIG WTG	Parameters	Wind Turbine	Parameters
L-L Voltage	575 V	Rotor Diameter	82.5 m
Rated Power	1.5 MW	Capacity Factor	52
Power Factor	0.9	Swept Area	5346 m2
Frequency	60 Hz	Rated Speed	12.5 m/s
Stator Resistance	0.0706 pu	Cut-in Speed	3.5 m/s
Stator Reactance	0.171 pu	Cut-out Speed	20 m/s
Rotor Resistance	0.005 pu	Tower Height	70 m
Rotor Reactance	0.256 pu	No. of Blade	3
Magn. Inductance	2.9 pu	Reliability	98%
Inertia Constant	1.5 s	Power Control	Pitch Control

real-world distorted case studies as discussed in the next section.

VI. STUDIED WIND POWER PLANT

The real-world cases are recorded from 60 Hz, 150 MW Trent Mesa WPP in Texas which is owned by American Electric Power (AEP). The one-line diagram of the WPP is shown in Fig. 8, and is provided by the courtesy of AEP. As seen in the diagram, the WPP has total seven segments, each segment has different output level. All these segments consist of 100 General Electric (GE) 1.5 MW type 3 (DFIG) wind turbine generators (WTGs), totaling 150 MW output power of the plant. The plant is connected via five circuits and 34.5/138 kV step-up transformers at 138 kV POI. Parameters of the GE 1.5 MW DFIG are provided in Table 3, and more details can be found in [30], [31]. Three types of disturbances are recorded at 138 kV POI of the Trent Mesas WPP-voltage sag, transient and oscillatory type. Only three-phase voltage and current signals are measured and sampling frequency of the signals is 7678.99 Hz. Using the recorded voltage and current signals, TFA-based instantaneous indices are measured to verify if the WPP meets the grid code requirements. The data are provided by the courtesy of National Renewable Energy Laboratory (NREL) in the US.

A. VOLTAGE SAG CASE STUDY

Voltage sag in electric power systems is typically caused by lightning and faults. Sudden change of load or excessive load can also be sources of voltage sag. Such a voltage sag and corresponding currents signals recorded at POI of Trent Mesa WPP are shown in Figs. 9(a) and (b), respectively. Results of voltage sag case study are summarized in Fig. 10 based on the TFA-based indices for wind power grid codes.

Fig. 10(a_1) shows the effective RMS voltage at POI stays above 0.9 pu both in steady-state and during the sag. Since pu RMS voltage always stays above LVRT curve discussed earlier, the WPP meets the first grid code requirement by FERC. Also, it is noticed that pu RMS voltage in steady-state (before and after the fault is cleared) is close to 1 pu. That lies within the voltage profile set point (0.95 pu to 1.05) by FERC and ERCOT. As seen in Fig. 10(a_2), the power factor is lagging or producing in steady-state and leading or absorbing during the voltage sag. In both conditions, power factor of the WPP is below 0.95 leading to 0.95 lagging, therefore, does not comply with the second grid code requirement issued by FERC.

According to IEEE Std. 519 [28], recommended voltage THD limit for $\mathbf{61}\boldsymbol{kV} < \boldsymbol{V} \leq \mathbf{161}\,\boldsymbol{KV}$ is 2.5%, where V is bus voltage at POI. The POI voltage in this study is 138 kV. Since the effective voltage THD in Fig. 11(a_3) is above 2.5% both in steady-state and transient conditions, the WPP does not comply with IEEE Std. 519 in this case study. The current THD limit in IEEE Std. 519 is provided based on short circuit ratio (SCR) at POI. SCR at POI of the Trent Mesa WPP is not provided or unknown. Hence, in this work, it is not possible to verify if the WPP meets the current THD limit as recommended in the standard. The current THD in Fig 11(a_4) decreases during the sag and is approximately 16%. The current THD decreases as fundamental component of current signal increases during the sag as observed in Fig. 9. In steady-state, the WPP delivers approximately 5 MW power to the grid whereas 40 MW power flows from grid to the WPP during sag as observed in Fig. 10 (b_3). Since, power delivered by the WPP is less than 10% (15 MW) of its nameplate capacity (150 MW), it may be disconnected from the grid according to ERCOT planning criteria for WPPs. It is also noticed, positive sequence active power $\mathbf{P_1^+}$, and harmonic active power $\mathbf{P_H}$ flow from grid to the WPP as shown in Figs. 10(b_1)-(b_2), respectively.

When reverse power flows, a WPP starts to operate as motor where turbine or prime mover acts as an active load. This reverse power flow may result in mechanical damage of wind generating units in the power plant. Therefore, it is necessary to clear the fault or disconnect the WPP from the grid once reverse power flow is detected. The effect of

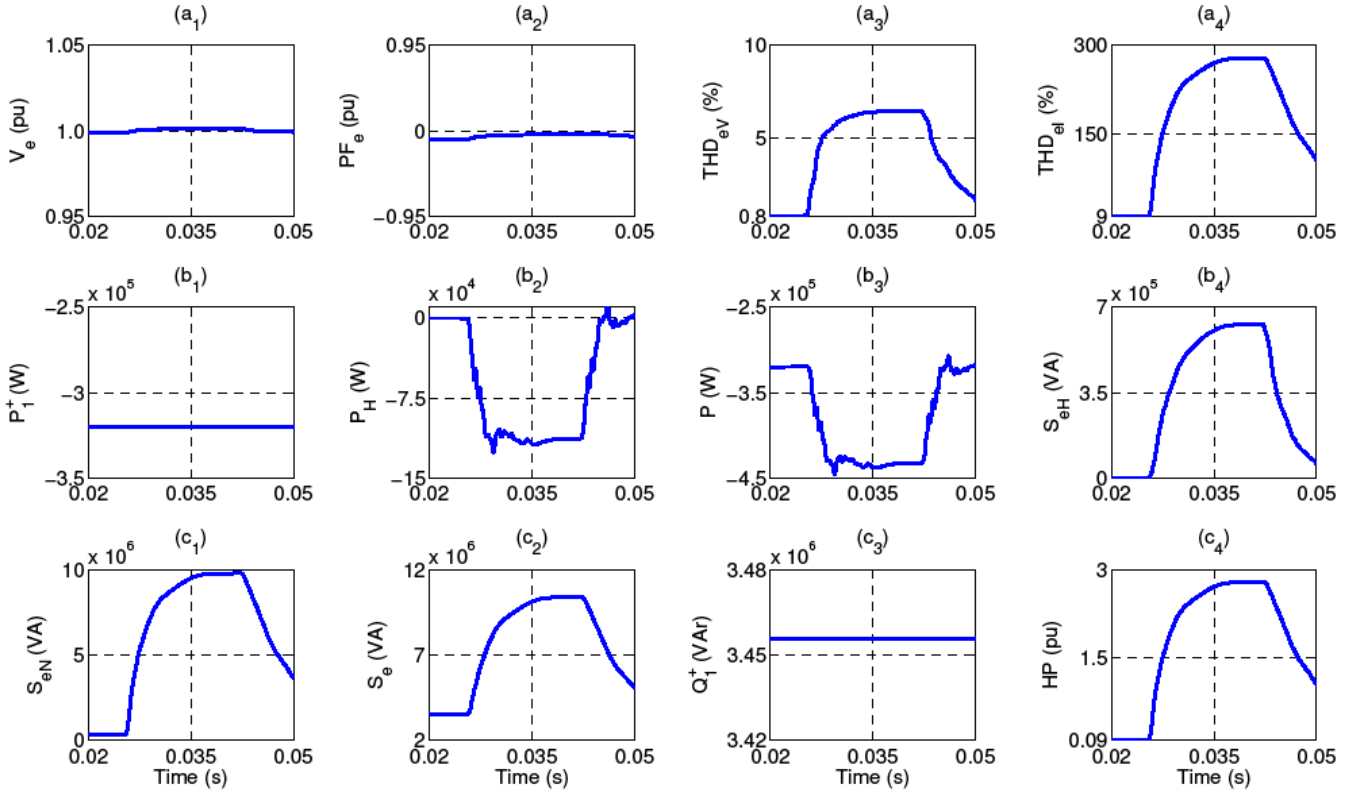

FIGURE 12. Results of transient case study analysis based on the proposed TFA technique for wind power grid codes in the US.

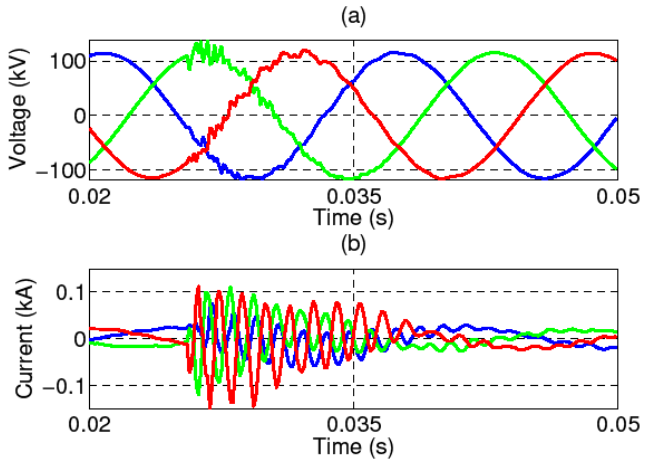

FIGURE 13. (a) Oscillatory voltage, and (b) corresponding current signal recorded from Trent Mesa WPP in Texas, US.

reverse power flow can further be mitigated by varying the penetration level of power units, by changing the protection relay settings to isolate the system and by implementing energy storage batteries to confine the reverse flow of power [32], [33]. The effective harmonic apparent power $\boldsymbol{S_{eH}}$, non-fundamental apparent power $\boldsymbol{S_{eN}}$, and total apparent power $\boldsymbol{S_e}$, of the WPP are summarized in Figs. 10(b_4), (c_1) and (c_2), respectively. The total apparent power of the WPP is increased to approximately 140 MVA during the fault as seen in Fig. 10(c_2). In steady-state, WPP delivers 5 MVAr reactive power to the grid, and lies within required reactive power range from −49.2 MVAr to 49.2 MVAr (32.8% of 150 MW capacity) as specified by ERCOT. However, during the sag, WPP operates at leading or absorbing power factor. Approximately 90 MVAr reactive power flows from grid to the WPP as observed in Fig. 10(c_3) and exceeds the required reactive power limit. Under this condition, ERCOT may require the WPP to disconnect from the grid [25]. Fig. 10(c_4) shows that harmonic pollution injected by the Trent Mesa WPP into 138 kV grid is above 0.12 pu.

B. TRANSIENT CASE STUDY

A WPP plant may introduce transient into the system when it is connected to or disconnected from the grid due to planned maintenance outage, or due to the switching of capacitors. Such a transient voltage and respective current signals that are recorded from Trent Mesa WPP are incorporated in Figs. 11(a) and (b), respectively.

The results of transient case study are provided in Fig. 12, and summarized in the following contexts. Fig. 12(a_1) shows that transient disturbance causes overvoltage at the POI. However, the effective RMS voltage $\boldsymbol{V_e}$ is above 0.9 pu both in normal and transient operating conditions, and meets the first wind power grid code requirement. The effective power factor $\boldsymbol{PF_e}$ in Fig. 12(a_2) is lagging or producing and above 0.95 pu. Hence, reliability of the WPP is not compromised

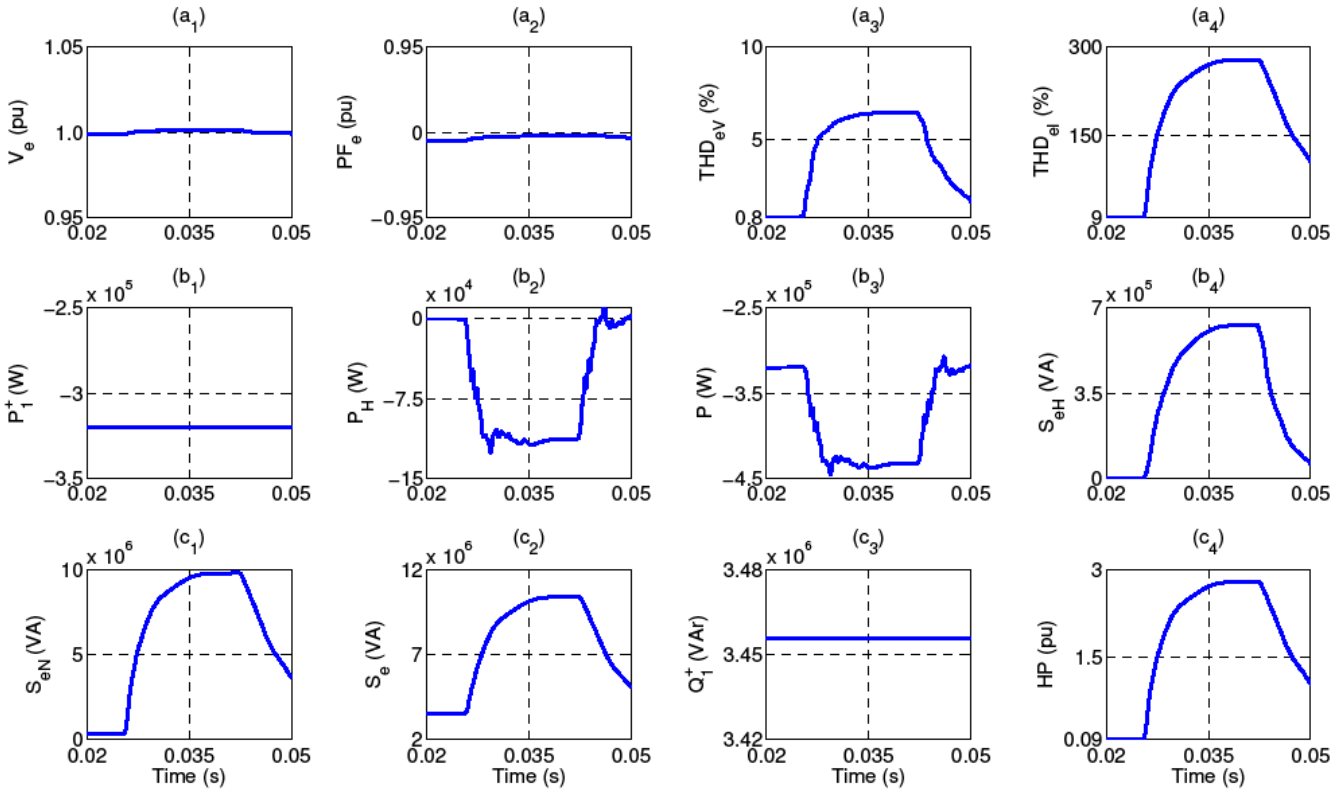

FIGURE 14. Results of oscillatory case study analysis based on the proposed TFA technique for wind power grid codes in the US.

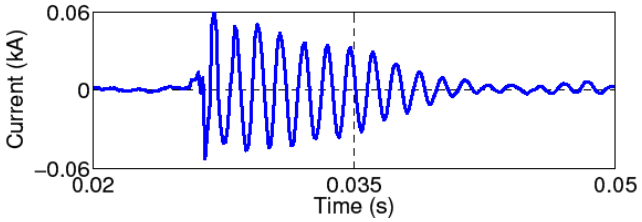

FIGURE 15. Decomposed phase A oscillatory current signal to identify the resonant frequency.

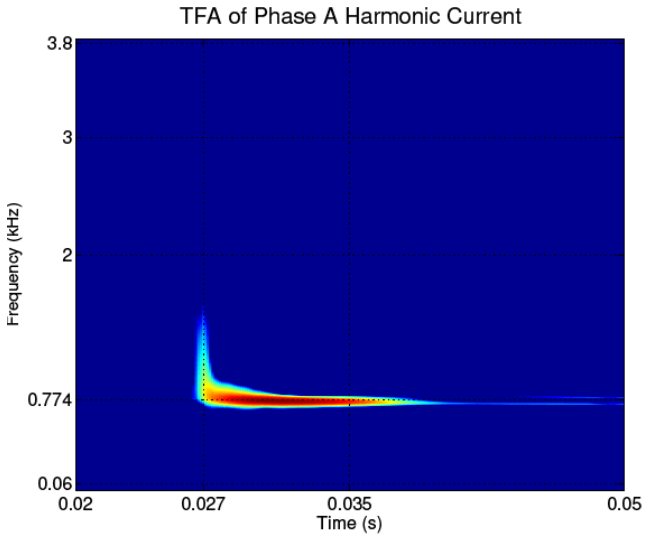

FIGURE 16. TFA of the phase A harmonic current demonstrates that 774 Hz resonant frequency appears at 0.027 s approximately.

by the transient disturbance according to the second grid code requirement issued by FERC. Figs. 12(a_3) and (a_4) illustrate that the transient disturbance increases the effective voltage and current THDs to approximately 10% and 4%, respectively during the transient condition, and the voltage THD is above the limit 2.5% as recommended in IEEE Std. 519 for 138 kV POI. The increase in the THDs is due to the high frequency components that are introduced by the transient disturbance into the system.

Unlike the voltage sag, in case of the transient case study, both the positive sequence active power $\boldsymbol{P}_1^+$ and total active power P flow from the WPP to the grid as seen in Figs. 12(b_1) and (b_3), respectively. The total active power delivered by the WPP into the grid is almost 112.3 MW, and is above 10% of the nameplate capacity as required by ERCOT. Also, the harmonic active power $\boldsymbol{P_H}$ is zero approximately in steady-state. However, it is increased during the transient due to the presence of high frequency component, and it flows from grid to the WPP as observed in Fig. 12(b_2). Figs. 12(b_4)-(c_2) illustrate that the apparent power of the WPP are increased by the transient disturbances. The positive sequence reactive power of the WPP is leading or absorbing,

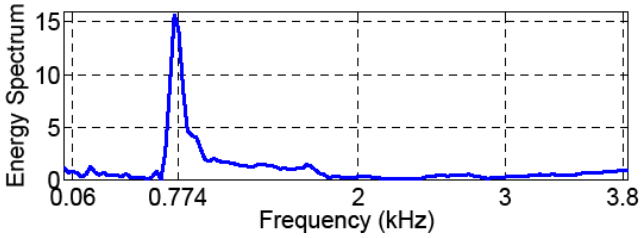

FIGURE 17. FFT of phase A harmonic shows the presence of 774 Hz resonant frequency only.

and approximately 10.5 MVAr reactive flows from grid to the WPP as seen in Fig. 12(c_3). This reactive power is within the range of −49.2 MVAr to +49.2 MVAr according to ERCOT reactive power requirement. Fig. 12(c_4) shows that the transient disturbance increases the harmonic pollution injection into the grid to 0.1 pu approximately due to the presence of transient frequency components.

Based on above discussion, it is summarized that the Trent Mesa WPP fulfills the 1st and 2nd grid code requirements by FERC. Also, it delivers more than 10% of the nameplate MW capacity, and absorbs 10.5 MVAr reactive power that lies within the recommended range from −49.2 MVAr to 49.2 MVAr. The plant also maintains the voltage profile set point as required by ERCOT. However, voltage THD is not within the limit as recommended by IEEE Std. 519.

C. OSCILLATORY CASE STUDY

A WPP typically consists of vast underground cables, reactive compensation equipment, transformers, and wind turbine generators with internal power factor correction capacitors. The energy exchange between inductive and capacitive elements of a WPP may lead to harmonic resonance and introduce oscillatory type disturbance into the grid. Figs. 13(a)-(b) represent such an oscillatory type voltage and a current disturbance waveforms recorded from the Trent Mesa wind generating plant. The corresponding TFA-based results are summarized in Fig. 14, and the following perceptions are made based on the case study analysis.

In oscillatory case study, the effective RMS voltage in Fig. 14(a_1) is above 0.9 pu, accordingly, the WPP fulfills the first grid code requirement. However, it shows very poor energy efficiency as the effective power factor in Fig. 14(a_2) is leading or absorbing, and close to zero. Thus, the WPP fails to meet the required power factor criteria according to the second grid code. Figs. 14(a_3)-(a_4) illustrate that both effective voltage THD and current THD increase during the oscillation. The voltage THD is above IEEE recommended limit of 2.5%. The current THD increases relatively to a high value (300% approximately) due to the presence of large magnitude of resonant frequency. In order to identify the resonant frequency, oscillatory frequency component of phase A current signal is decomposed, and incorporated in Fig. 15. The time frequency distribution of the decomposed signal is shown in Fig. 16. Fig. 16 demonstrates that 774 Hz

TABLE 4. Summary of real-world case study analyses.

SCADA DATA	Indices	Volt. Sag	Tran.	Osc.
RMS Volt. (pu)	V_e	0.9556	1.002	1.0002
Power Factor (pu)	PF_e	0.1136	0.9937	-0.0576
THD%	THD_{eV}	6.990	4.567	4.234
	THD_{e1}	35.18	2.010	174.7
Active Power (MW)	P_1^+	-12.96	112.23	-0.3203
	P_H	-0.1590	-0.0319	-0.0622
	P	-12.34	112.27	-0.3816
Apparent Power (MVA)	S_{eH}	0.9755	0.1469	0.3353
	S_{eN}	13.51	5.731	6.136
	S_e	62.79	112.98	7.462
Reactive Power (MVAr)	Q_1^+	-33.34	-10.61	3.456
Harmonic Pollution (pu)	HP	0.3634	0.0508	1.751
Grid Codes	LVRT	Yes	Yes	Yes
	PF	No	Yes	No
	THD	No	No	No
	Q	Yes	Yes	Yes
	P	No	Yes	No

is responsible harmonic resonance issue in the WPP. This energy of this resonant frequency appears at $t = 0.027s$ approximately, and decreases as the oscillation dies out with time. Whereas, FFT in Fig. 17 shows the presence of 774 Hz resonant frequency only, and does not provide time information of the resonant frequency as TFA does. Small amount of positive sequence active power P_1^+, harmonic active power P_H and total active power P flow from grid to the WPP as seen in Figs. 15(b_1)-(b_3), respectively. Further, the oscillatory disturbance increases the harmonic and non- fundamental apparent power from 0 to 0.7 MVA and 10 MVA, respectively as observed in Figs. 14(b_4)-(c_1).

Fig. 14(c_3) represents the positive sequence reactive power is constant, and flows from WPP to the grid. Also, oscillatory disturbance causes the harmonic pollution to increase to a relatively high value of 3 pu approximately compared to previous two case studies. In this case study, WPP maintains required voltage profile at POI and reactive power is within the defined range (−49.2 MVAr to 49.2 MVAr) set the by ERCOT. However, the WPP fails to meet required power criteria and deliver 10% (15 MW) of the nameplate MW capacity. The results of case studies are summarized in Table 4. As seen in the table, the effective RMS voltage is above 0.9 pu in all three case studies. Therefore, WPP meets the first grid code requirement by FERC. The required power factor at POI is maintained in transient case study only which is 0.9937 pu lagging or producing. In all three cases, voltage THD is not within the limit of 2.5% at POI. Further, according to ERCOT planning criteria, reactive power at POI is within the range of −49.2 MVAr to 49.2 MVAr in all three cases. And, the WPP delivers more than 10% (15 MW) active power to the grid in transient case study only.

Thus, this research work provides detailed analysis of Trent Mesa WPP in accordance with wind power grid codes

compliance under unbalanced and distorted grid conditions. That researchers may find beneficial for further interconnection study of WPPs into the grid.

VII. CONCLUSION

In this work, a new time-frequency analysis (TFA) method has been proposed for analysis of wind power grid codes in the US under unbalanced and distorted grid conditions. Using the TFA technique, a set of indices have been redefined for wind power grid codes utilizing Time-Frequency Toolbox (TFTB) in MATLAB®. The efficacy of the proposed method has been justified by employing it to computer simulated and real-world unbalanced and distorted case studies. Results of the computer simulated case studies have justified that TFA-based proposed method provides much more accurate results than the classical FFT under non-stationary, non-sinusoidal and unbalanced conditions. Also, analysis of real-world case studies has demonstrated that TFA-based redefined indices are able to verify WPP grid code requirements effectively. In addition, TFA-based redefined indices have extracted dynamic signature of the disturbances for WPP SCADA system. For example, it has detected reverse power flow where disconnection of the WPP is required to protect power system reliability. Also, in oscillatory case study, the TFA technique has identified the time varying harmonic resonant frequency that is responsible for oscillation into the system. Thus, the proposed method could be used not only for instantaneous verification of wind power grid code requirements, but also for providing useful information to WPP SCADA system from power system reliability perspectives.

REFERENCES

[1] *20% Wind Energy by 2030*, document DOE/GO-102008-2567, Dept. Energy, United States Amer., Jul. 2008.

[2] M. Tsili and S. Papathanassiou, "A review of grid code technical requirements for wind farms," *IET Renew. Power Gener.*, vol. 3, no. 3, pp. 308–332, Sep. 2009.

[3] H. H. Abdeltawab and Y. A.-R.-I. Mohamed, "Robust energy management of a hybrid wind and flywheel energy storage system considering flywheel power losses minimization and grid-code constraints," *IEEE Trans. Ind. Electron.*, vol. 63, no. 7, pp. 4242–4254, Jul. 2016.

[4] M. N. I. Sarkar, L. G. Meegahapola, and M. Datta, "Reactive power management in renewable rich power grids: A review of grid-codes, renewable generators, support devices, control strategies and optimization algorithms," *IEEE Access*, vol. 6, pp. 41458–41489, 2018.

[5] C. Sourkounis and P. Tourou, "Grid code requirements for wind power integration in Europe," in *Proc. Conf. Papers Energy*, 2013, pp. 1–9.

[6] Y. Yang, P. Enjeti, F. Blaabjerg, and H. Wang, "Suggested grid code modifications to ensure wide-scale adoption of photovoltaic energy in distributed power generation systems," in *Proc. IEEE Ind. Appl. Soc. Annu. Meeting*, Oct. 2013, pp. 1–8, doi: 10.1109/ias.2013.6682485.

[7] *Federal Energy Regulatory Commission (FERC), United States of America, Docket No. RM05-4-001; Order No. 661-A, Interconnection for Wind Energy*. Accessed: Dec. 12, 2005. [Online]. Available: https://www.ferc.gov/EventCalendar/Files/20051212171744-RM05-4-001.pdf

[8] *Federal Energy Regulatory Commission (FERC), United States of America, Docket No. RM 16-1-000; Order No. 827, Reactive Power Requirements for Non-Synchronous Generation*. Accessed: Jun. 16, 2016. [Online]. Available: https://www.ferc.gov/whats-new/comm-meet/2016/061616/E-1.pdf

[9] K.-J. Du, X.-Y. Xiao, Y. Wang, Z.-X. Zheng, and C.-S. Li, "Enhancing fault ride-through capability of DFIG-based wind turbines using inductive SFCL with coordinated control," *IEEE Trans. Appl. Supercond.*, vol. 29, no. 2, pp. 1–6, Mar. 2019.

[10] Y. M. Alsmadi, L. Xu, F. Blaabjerg, A. J. P. Ortega, A. Y. Abdelaziz, A. Wang, and Z. Albataineh, "Detailed investigation and performance improvement of the dynamic behavior of grid-connected DFIG-based wind turbines under LVRT conditions," *IEEE Trans. Ind. Appl.*, vol. 54, no. 5, pp. 4795–4812, Sep. 2018.

[11] M. Firouzi and G. B. Gharehpetian, "LVRT performance enhancement of DFIG-based wind farms by capacitive bridge-type fault current limiter," *IEEE Trans. Sustain. Energy*, vol. 9, no. 3, pp. 1118–1125, Jul. 2018.

[12] *Technical Analysis of the August 14, 2003, Blackout: What Happened, Why, and What Did We Learn?* North Amer. Electr. Rel. Council, Atlanta, GA, USA, Jul. 20014.

[13] M. Islam, H. A. Mohammadpour, A. Ghaderi, C. W. Brice, and Y.-J. Shin, "Time-frequency-based instantaneous power components for transient disturbances according to IEEE standard 1459," *IEEE Trans. Power Del.*, vol. 30, no. 3, pp. 1288–1297, Jun. 2015.

[14] R. Duan and F. Wang, "Fault diagnosis of on-load tap-changer in converter transformer based on time–frequency vibration analysis," *IEEE Trans. Ind. Electron.*, vol. 63, no. 6, pp. 3815–3823, Jun. 2016.

[15] T. Neumann, T. Wijnhoven, G. Deconinck, and I. Erlich, "Enhanced dynamic voltage control of type 4 wind turbines during unbalanced grid faults," *IEEE Trans. Energy Convers.*, vol. 30, no. 4, pp. 1650–1659, Dec. 2015.

[16] Y. Zhang, E. Muljadi, D. Kosterev, and M. Singh, "Wind power plant model validation using synchrophasor measurements at the point of interconnection," *IEEE Trans. Sustain. Energy*, vol. 6, no. 3, pp. 984–992, Jul. 2015.

[17] M. Islam, H. A. Mohammadpour, P. Stone, and Y.-J. Shin, "Time-frequency based power quality analysis of variable speed wind turbine generators," in *Proc. IECON 39th Annu. Conf. IEEE Ind. Electron. Soc.*, Nov. 2013.

[18] P. Stone, M. Islam, and Y.-J. Shin, "Power quality impact of wind turbine generators on the electrical grid," in *Proc. IEEE Energytech*, Cleveland, OH, USA, May 2012, pp. 1–6.

[19] B. Liu, Z. Li, X. Chen, Y. Huang, and X. Liu, "Recognition and vulnerability analysis of key nodes in power grid based on complex network centrality," *IEEE Trans. Circuits Syst., II, Exp. Briefs*, vol. 65, no. 3, pp. 346–350, Mar. 2018.

[20] S. Li, Y. Hu, L. Zheng, Z. Li, X. Chen, T. Fernando, H. H. C. Iu, Q. Wang, and X. Liu, "Stochastic event-triggered cubature Kalman filter for power system dynamic state estimation," *IEEE Trans. Circuits Syst., II, Exp. Briefs*, vol. 66, no. 9, pp. 1552–1556, Sep. 2019.

[21] X. Liu, L. Li, Z. Li, X. Chen, T. Fernando, H. H.-C. Iu, and G. He, "Event-trigger particle filter for smart grids with limited communication bandwidth infrastructure," *IEEE Trans. Smart Grid*, vol. 9, no. 6, pp. 6918–6928, Nov. 2018.

[22] S. Li, L. Li, Z. Li, X. Chen, T. Fernando, H. H.-C. Iu, G. He, Q. Wang, and X. Liu, "Event-trigger heterogeneous nonlinear filter for wide-area measurement systems in power grid," *IEEE Trans. Smart Grid*, vol. 10, no. 3, pp. 2752–2764, May 2019.

[23] S.-H. Cho, G. Jang, and S.-H. Kwon, "Time-frequency analysis of power-quality disturbances via the Gabor–Wigner transform," *IEEE Trans. Power Del.*, vol. 25, no. 1, pp. 494–499, Jan. 2010.

[24] M. Blodt, M. Chabert, J. Regnier, and J. Faucher, "Mechanical load fault detection in induction motors by stator current time-frequency analysis," *IEEE Trans. Ind. Appl.*, vol. 42, no. 6, pp. 1454–1463, Nov. 2006.

[25] H. A. Mohammadpour, M. M. Islam, E. Santi, and Y.-J. Shin, "SSR damping in fixed-speed wind farms using series FACTS controllers," *IEEE Trans. Power Del.*, vol. 31, no. 1, pp. 76–86, Feb. 2016.

[26] W. Cole, J. Kim, K. Kapoor, and T. Edgar, "Addressing the peak power problem through thermal energy storage," in *Case Studies in Operations Research* (International Series in Operations Research & Management Science), vol. 212. New York, NY, USA: Springer, 2014, doi: 10.1007/978-1-4939-1007-6_14.

[27] L. Cohen, *Time-Frequency Signal Analysis*. New York, NY, USA: Prentice-Hall, 1995.

[28] *IEEE Standard Definitions for the Measurement of Electric Power Quantities Under Sinusoidal, Nonsinusoidal, Balanced, or Unbalanced Conditions*, IEEE Standard 1459-2010, Mar. 2010.

[29] *ERCOT Nodal Protocols*, ERCOT, Austin, TX, USA, Apr. 2018.

[30] *Reliability Standards for the Bulk Electric Systems of North America*, North Amer. Electr. Rel. Corp., Atlanta, GA, USA, Jun. 2019.

[31] E. Muljadi, T. Tian, and M. Miller, "Comparison of standards and technical requirements of grid connected wind power plants in China and the United States," Nat. Renew. Energy Lab. (NREL), Lakewood, CO, USA, Tech. Rep. NREL/TP-5D00-64225, Sep. 2016.
[32] *IEEE Recommended Practice and Requirements for Harmonic Control in Electric Power Systems*, IEEE Standard 519-2014 (Revision of IEEE Std 519-1992), Jun. 2014, pp. 1–29.
[33] J. D. Glover, M. S. Sarma, and T. Overbye, *Power System Analysis and Design*, 5th ed. Boston, MA, USA: Cengage Learning, 2017, p. 379.
[34] G. O. Young, "Synthetic structure of industrial plastics," in *Plastics*, vol. 3, J. Peters, Ed., 2nd ed. New York, NY, USA: McGraw-Hill, 1964, pp. 15–64.
[35] N. Miller, J. Sanchez-Gasca, W. Price, and R. Delmerico, "Dynamic modeling of GE 1.5 and 3.6 MW wind turbine-generators for stability simulations," in *Proc. IEEE Power Eng. Soc. General Meeting*, vol. 3, Jul. 2003, pp. 1977–1983.
[36] K. N. Bangash, M. E. A. Farrag, and A. H. Osman, "Manage reverse power flow and fault current level in lv network with high penetration of small scale solar and wind power generation," in *Proc. 53rd Int. Univ. Power Eng. Conf. (UPEC)*, Glasgow, Scotland, Sep. 2018, pp. 1–6.
[37] S. Rahman, H. Aburub, M. Moghaddami, and A. I. Sarwat, "Reverse power flow protection in grid connected PV systems," in *Proc. SoutheastCon*, St. Petersburg, FL, USA, Apr. 2018, pp. 1–5.

MD MOINUL ISLAM (Member, IEEE) received the B.Sc. degree in electrical and electronic engineering from the Bangladesh University of Engineering and Technology (BUET), in 2007, and the M.E. degree in electrical engineering and the Ph.D. degree in power systems from the University of South Carolina, SC, USA, in 2011 and 2014, respectively. In 2015, he started working as a Postdoctoral Fellow and an Adjunct Faculty with the Department of Electrical Engineering, University of South Carolina, Columbia, SC, USA. Later, he joined the Electric Reliability Council of Texas ERCOT, TX, USA, in 2019. Since then, he has been working in Planning Engineering III as a member of the ERCOT Transmission Planning. His primary research interests include renewable energy sources, power quality, time–frequency analysis, and electric power system reliability issues.

EKLAS HOSSAIN (Senior Member, IEEE) received the B.S. degree in electrical and electronic engineering from the Khulna University of Engineering and Technology, Bangladesh, in 2006, the M.S. degree in mechatronics and robotics engineering from the International Islamic University of Malaysia, Malaysia, in 2010, and the Ph.D. degree from the College of Engineering and Applied Science, University of Wisconsin Milwaukee (UWM), in 2016. He has been working in the area of distributed power systems and renewable energy integration for last ten years and he has published a number of research papers and posters in this field. He is now involved with several research projects on renewable energy and grid tied microgrid system at Oregon Tech, as an Assistant Professor with the Department of Electrical Engineering and Renewable Energy, since 2015. His research interests include modeling, analysis, design, and control of power electronic devices; energy storage systems; renewable energy sources; integration of distributed generation systems; microgrid and smart grid applications; robotics, and advanced control system. He, along with his dedicated research team, is looking forward to explore methods to make the electric power systems more sustainable, cost-effective, and secure through extensive research and analysis on energy storage, microgrid system, and renewable energy sources. He is a Senior Member of the AEE. He is the winner of the Rising Faculty Scholar Award from the Oregon Institute of Technology, in 2019, for his outstanding contribution in teaching. He is currently serving as an Associate Editor of IEEE Access.

SANJEEVIKUMAR PADMANABAN (Senior Member, IEEE) received the bachelor's degree from the University of Madras, India, in 2002, the master's degree (Hons.) from Pondicherry University, India, in 2006, and the Ph.D. degree from the University of Bologna, Italy, in 2012. He was an Associate Professor with VIT University, from 2012 to 2013. In 2013, he joined the National Institute of Technology (Puducherry), India, as a Faculty Member. In 2014, he was invited as a Visiting Researcher at the Qatar University, Qatar, funded by the Qatar National Research Foundation (Government of Qatar), and also a Lead Researcher with the Dublin Institute of Technology, Ireland. He was an Associate Professor with the Department of Electrical and Electronics Engineering, University of Johannesburg, South Africa, from 2016 to 2018. Since March 2018, he has been a Faculty Member of the Department of Energy Technology, Aalborg University, Esbjerg, Denmark. He has authored over 350 scientific papers and has received the Best Paper cum Most Excellence Research Paper Award from the IET-SEISCON'13, IET-CEAT'16, and five Best Paper Award from ETAEERE'16 sponsored Lecture note in Electrical Engineering, Springer book series. He is involved as a member on the invitation with various capacities in committees for several international conferences, including the IEEE and the IET. He is a Fellow of the Institute of Electronics and Telecommunication Engineers (FIETE), India, and a Fellow of the Institute of Engineers (FIE), India. He serves as an Editor/Associate Editor/Editorial Board of many-refereed journal, in particular, the IEEE Systems Journal, the IEEE Access Journal, the *IET Power Electronics*, and the Subject Editor of the *IET Renewable Power Generation*, the Subject Editor of the *IET Generation, Transmission and Distribution*, the *FACTS Journal* (Canada), and the *Journal of Power Electronics* (South Korea).

CHARLES W. BRICE received the B.E.E., M.S.E.E., and Ph.D. degrees in electrical engineering from the Georgia Institute of Technology, Atlanta, GA, USA, in 1971, 1972, and 1977, respectively. He is currently an Associate Professor with the Department of Electrical Engineering, University of South Carolina, Columbia, SC, USA. He was a member of the faculty of the Department of Electrical Engineering, Texas A&M University, College Station, TX, USA, from 1977 to 1983. His fields of interests are modeling and simulation of electric power systems, controls, and electric machines and drives.